Dyes and Pigments 196 (2021) 109758

Contents lists available at ScienceDirect

Dyes and Pigments

journal homepage: www.elsevier.com/locate/dyepig

An aggregation-induced emission (AIE)-active fluorescent chemodosimeter for selective sensing of hypochlorite in water and solid state: Endogenous detection of hypochlorite in live cells

Sandip Kumar Samanta [a], Kalipada Maiti [a], Saikat Kumar Manna [b], Syed Samim Ali [a], Uday Narayan Guria [a], Aritri Ghosh [c], Pallab Datta [c], Ajit Kumar Mahapatra [a,*]

[a] Department of Chemistry, Indian Institute of Engineering Science and Technology, Shibpur, Howrah, 711103, India
[b] Department of Chemistry, Haldia Government College, Debhog, West Bengal, 721657, India
[c] Centre for Healthcare Science and Technology, Indian Institute of Engineering Science and Technology, Shibpur, India

ARTICLE INFO

Keywords:
AIE
Turn-on chemodosimeter
Hypochlorite (ClO^-)
Theoretical study
Solid state sensing
Real water sample analysis
Cell imaging

ABSTRACT

Hypochlorite (ClO^-) being an important reactive oxygen species plays a crucial role in the oxidative damage to tissue and other various diseases. Highly selective, sensitive, and quick detection of aberrant ClO^- is vital for the protection of living organisms and the environment. Accordingly, fluorescent molecules are most effective sensor system for ClO^-. Herein, we have synthesized and characterized a water soluble AIE-active tetraphenylethylene (TPE)-based fluorescent molecule TPE−Py^+ (**TPP**) for rapid (10 s) and selective detection of ClO^- based on ClO^- induced oxidation of N-alkylpyridinium to N-methyl-2-pyridone. ClO^- mediated aggregation-induced emission (AIE) enhancement corresponds to turn-on response. Scanning electron microscopic (SEM) study supports AIE behavior of the probe upon treatment with ClO^-. The detection limit of **TPP** for ClO^- was found to be 8.89 nM and exhibited high selectivity among other possibly interfering analytes (ROS, RNS, other ions). **TPP**-based handy test kits were developed for the solid-state detection of ClO^- in environmental samples. Furthermore, our probe was effective in detecting ClO^- in real water samples, fetal bovine serum and able to detect endogenous ClO^- in live cell.

1. Introduction

Recent research suggests that the elevated reactive oxygen species (ROS) production promotes both viral replication and monocyte activation. Coronavirus infection increase the oxidative stress which increase the concentration of ROS which can oxidize the cysteine residues on the peptide domain of Angiotensin-Converting Enzyme 2 (ACE2) receptors and RBD (receptor binding domain) of SARS-CoV kept them in oxidized forms (disulphide), rather than reduced form (thiol). It looks convincible that oxidation of these thiol to disulfides, during oxidative stress, would rise the rapport of SARS-CoV-2 proteins for the ACE2 receptor, and thus, enhance the seriousness of COVID-19 poison. Enhanced oxidative stress may accompanied with endothelial affliction and community inflammation, that put up to acute lung injury, thrombosis, cytokine storm and found in serious COVID-19 sickness [1–5].

Among the several ROS, hypochlorous acid (HClO)/hypochlorite (ClO^-) is frequently utilized as an influential bleaching agent in our daily lives and as a primary antimicrobial agent in the natural immune system [6,7]. Due to strong oxidizing effect of ClO^-, it would resistance the invasion of bacteria and regulates the lifecycle in the cell. The workable level of ClO^- in the living body is essential to human health, whereas excessive ClO^- production from phagocytes can influence inflammation-related tissue injury and various diseases, including severe liver injury, rheumatoid arthritis, peritonitis, cardiovascular diseases, atherosclerosis, neuron degeneration, pulmonary lesions and even cancers [8–18]. Endogenous ClO^- can be produced by the peroxidation reaction of H_2O_2 (hydrogen peroxide) and Cl^- (chloride ion) catalyzed by the MPO (myeloperoxidase) in triggered leukocytes such as monocytes, macrophages, and neutrophils [19,20]. As a result, it is essential to effectively identify ClO^- in living systems for medical diagnosis and therapy.

A number of conventional analytical techniques are developing to detect ClO^- but fluorescence spectroscopy technique is the best techniques since its good selectivity, low detection limit, sensitivity, cost-

* Corresponding author.
E-mail address: akmahapatra@chem.iiests.ac.in (A.K. Mahapatra).

https://doi.org/10.1016/j.dyepig.2021.109758
Received 25 June 2021; Received in revised form 27 August 2021; Accepted 27 August 2021
Available online 28 August 2021

effective, non-destructive nature, fastness and reliability [21]. Fluorescence bio imaging based on small-molecule fluorescent probes is becoming research hot topic [22–24]. To date, many fluorescent probes have been developed to detect ClO^-, including pyrene, BODIPY (borondipyrromethene), benzothiazole, rhodamine, coumarin and cyanine [25–37]. Generally, these fluorescence sensors suffered from severe limitations such as long response time, working in high pH condition, excitation or emission in the ultraviolet region, fair photostability. Eventually, many of them suffer from an ACQ (aggregation-caused quenching) owing to the π- π* stacking interactions and it is potent in the solid state or, in a large number of organic solvents, limiting the real applications in biological systems [38–42].

Till date, lots of fluorescent sensors for ClO^- have been reported but still there are some opportunity to construct a fluorescence sensor of ClO^- to develop performance there by optimizing the recognition moiety which upon reactions with ClO^-, may deliver intensified fluorescence distinction. Shen et al. have reported a mitochondria-targeted coumarin–pyridine derivative (CPD) for ClO^- through dual fluorescence emission peaks [43]. Again Wu et al. have reported pyrene derivative (Py-Cy) for ClO^- through cleavage of the double bond [44]. Generally, their design strategies are based on oxidation of thioether to sulfonate [45–49], deprotection [50–52], oxidation of phenol to quinone [53–55], oxime to aldehyde [56,57] and C=C bond to aldehyde [58,59]. Again Liu et al. have reported a deep-red AIE-active fluorophore for ClO^- [60]. But these probes showed specific turn-off fluorescent-response. Recently, Wang et al. have reported a TPE based fluorescent probe for ClO^- through cleavage of the Py^+-N group [61].

With the aforementioned concerns in mind, herein, we report a new Tetraphenyl ethylene (TPE) conjugate N-alkyl pyridinium ion (**TPP**) for sensing OCl^- with significant aggregation-induced fluorescence enhancement in aqueous solution. TPE was chosen as AIEgen, as it has been applied in biological imaging and hold good photo-stability [62–64]. Quaternized pyridine have been employed with TPE to extent the emission wave length. Again, quaternized pyridine moiety is mitochondria-targeted functional groups [65–67] and able to improves compound's water solubility considerably. In this work, ClO^- oxidizes N-alkyl pyridinium moiety to N-methyl-2-pyridone and then the hydrophobicity of the probe is changed which is accompanied with aggregation-induced emission enhancement. Scanning electron microscopy (SEM) study revealed that oxidation of N alkyl pyridinium to N-methyl-2-pyridone influences the aggregation of AIEgens. The probe exhibited good selectivity, rapid response, and high sensitivity to ClO^- over other ROS and ions. Interestingly, **TPP** can be applied for detection of ClO^- in fetal bovine serum sample. Furthermore, **TPP** can detect ClO^- in live MG63 (osteosarcoma – human) and MC3T3 (osteoblast – mouse) cells. The results of this effort are described below.

2. Results and discussion

2.1. Synthesis of the probe

Synthetic procedure of sensor for ClO^- (**TPP)** is quite simple. Desire compound **TPP** can be conveniently synthesized by condensation of TPE-CHO with N-methyl-4- methyl-Pyridium iodide under the catalysis of piperidine, affording the target product in a good yield (Scheme 1). Structural characterization of the probe **TPP** was characterized by HRMS spectroscopy, ^1H NMR, and ^{13}C NMR (Figs. S5–S7).

2.2. Absorption spectra responses of TPP towards ClO^-

Photophysical properties of the probe was studied in PBS buffer (pH = 7.4, 10.0 mM, 0.1% DMSO, 25 °C) solution. NaClO was employed as the standard ClO^- source in the entire photophysical study. UV–visible spectral measurement of the probe **TPP** (1.0 μM) exhibited an absorbance band at 386 nm. With the addition of 3.2 equiv. ClO^-, the peak at 386 nm was progressively quenched and a new peak at 292 nm was increased steadily. An isosbestic point was observed at 330 nm, indicating that a chemical reaction occurred, which was concomitant with the production of a novel N-methyl-2-pyridone compound. As a result of the inhibition of the ICT process from TPE to pyridinium moiety, a hypsochromic shift was found in absorption spectra.

Eventually, an apparent naked eye colour transformation from yellow to colourless was observed (Fig. 1), allowing for the identification of ClO^- in environmental samples through the naked eye.

2.3. Fluorescence response of the probes to ClO^-

Next, motivated by the distinctive UV–vis spectrum, we investigated the emission spectra of probe for ClO^- under the same condition. The probe **TPP** generated a very weak emission at ~522 nm (Φ = 0.021) when excited at 400 nm in PBS buffer (pH = 7.4, 10 mM, 0.1% DMSO, pH = 7.4, 25 °C) solution. With an increase in ClO^- concentration, the

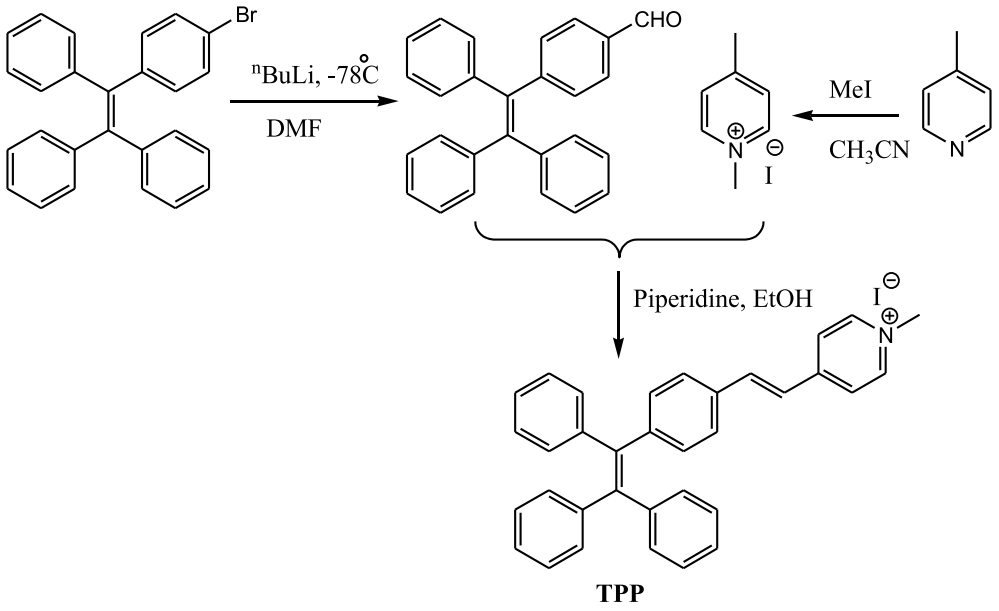

Scheme 1. The Synthetic procedure of chemodosimeter **TPP.**

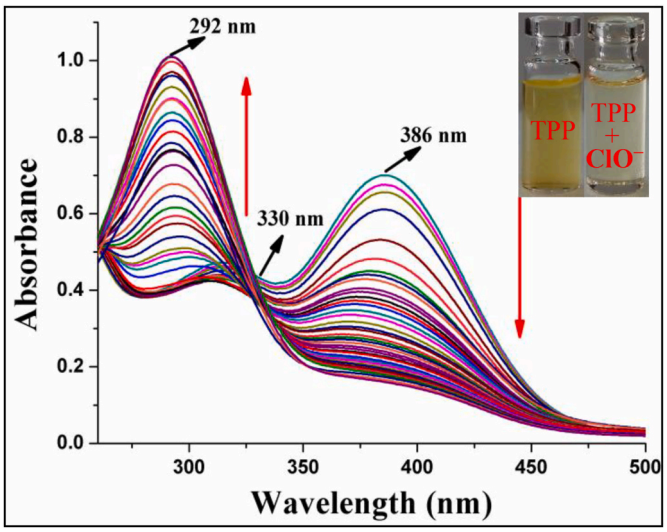

Fig. 1. Absorption spectra of **TPP** (1.0 μM) upon addition of ClO^- in PBS buffer solution (10.0 mM, pH = 7.4, at 25 °C).

emission intensity of the probe **TPP** at 544 nm (Φ = 0.25) increased significantly (10-fold), emission intensity reached maximum after the addition of 3.2 equiv. of ClO^- (Fig. 2). Initially the probe is nonfluorescent in PBS solution due to aggregation caused quenching (ACQ). Probe **TPP** have a propensity to aggregate when they move from the organic to the aqueous phases, increasing the possibility of collisions between molecules and resulting in energy loss, resulting in fluorescence quenching.

However, **TPP** showed strong yellow fluorescence with gradual addition of ClO^-. Interestingly a nonemissive probe showed a "turn-on" response due to the oxidation of N-alkylpyridinium moeity to N-methyl-2-pyridone moiety in presence of ClO^-. Since hydrophobicity of the probes is changed as a result increased aggregation-induced emission (AIE).

Furthermore, a linear relationship (at 544 nm) with ClO^- concentration range of 0–0.3 μM was observed with a relationship coefficient of $R^2 = 0.99237$ (Fig. S3a). The detection limit of ClO^- was calculated to be 8.9 nM (Fig. S11). The results of time-dependent fluorescence response studies are displayed in Fig. S3b. The probe **TPP** had a low intensity fluorescence band that was enhanced by 3.0 equiv. ClO^- and reached plateau within 10 s. The pseudo-first order rate constant k = 0.01878 sec^{-1} (Fig. S4). **TPP** displayed outstanding response time and a lesser detection limit, which might be appreciated in sensitive, real-time monitoring of ClO^- in living systems.

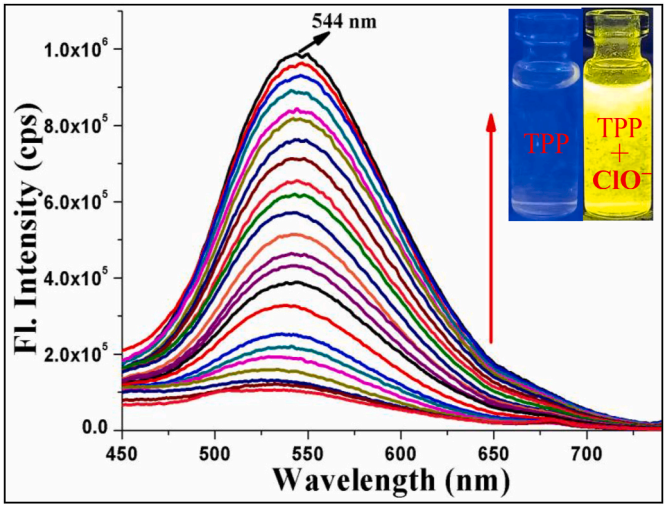

Fig. 2. Fluorescence spectra of **TPP** (1.0 μM) at λ_{ex} = 400 nm, upon addition of ClO^- in PBS buffer (10.0 mM, pH = 7.4, at 25 °C) solution.

2.4. Fluorescence lifetime studies of the TPP

Time resolved fluorescence experiments were performed to assess the AIE tendency of **TPP** before and after addition of ClO^-. This experiment displayed a significant increase in lifetime in presence of ClO^- ions (Fig. 3). The average lifetime was calculated to be 1.68 ns for **TPP** only and 35,889 ns after addition of ClO^- ions, using the standard method. Results suggested a slower tri -exponential (ℓ3) decay for probe **TPP** emission (Tables S3 and SI). To evaluate the AIE effect, lifetime in case of **TPP** + ClO^- has been determined which was more delayed and also tri-exponential (ℓ3).

These results conclude that by adding ClO^-, the decay of the excited state was much slower i.e., remain for much time, which evidently described the presence of AIE phenomenon [68] (Fig. 3).

2.5. SEM study

To get inside in to the aggregation behaviour of the probe scanning electron microscope (SEM) study were carried out. SEM image of **TPP** in PBS buffer displayed small spherical aggregates (Fig. 4a, b, c). Whereas upon addition of ClO^- self-assembled big spherical aggregates were observed (Fig. 4d, e, f). These studies suggest the change in the morphology and increase in size of the aggregates in the presence of ClO^- was due to self-aggregation of AIE-gen. This study also revealed that size of **TPP** molecule was in the range of 68–230 nm (Fig. S12a, Table S4). Whereas, size of the molecules increased (320–540 nm) upon treatment with of ClO^- (Fig. S12b, Table S4). It is believed that the limitation in intramolecular rotation (RIR) and aggregation-driven development is the major cause of the fluorescence enhancement [69].

2.6. Selectivity and specificity of TPP

Unlike ROS (reactive oxygen species), RNS (reactive nitrogen species) and RSS ((reactive sulphur species) were chosen to study the selectivity of **TPP**. As estimated, compared with ClO^- no apparent fluorescence changes were observed when probe **TPP** was incubated with various competitive species, including H_2S, CH_3CO_3H, NO, $ONOO^-$, •OH, $^1O_2$, O^{2-}, GSH (glutathione), SO_3^{2-}, H_2O_2 (Fig. 5a). and furthermore, no fluorescence alteration was perceived for different

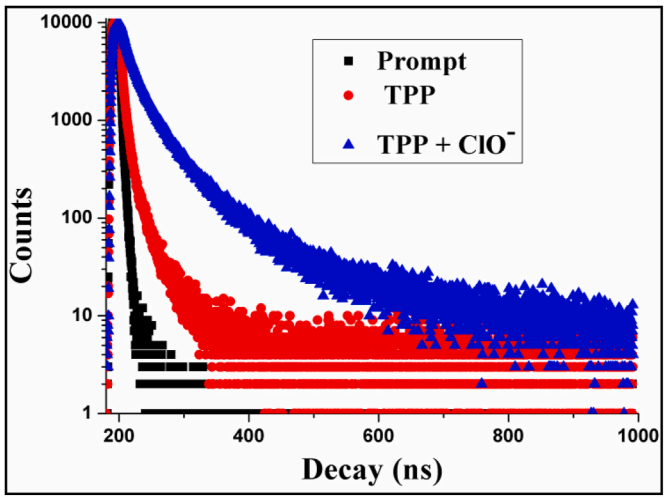

Fig. 3. Red dot represents fluorescence lifetime decays of **TPP** and blue dot represents fluorescence lifetime decays of after addition of ClO^- in PBS buffer solution.

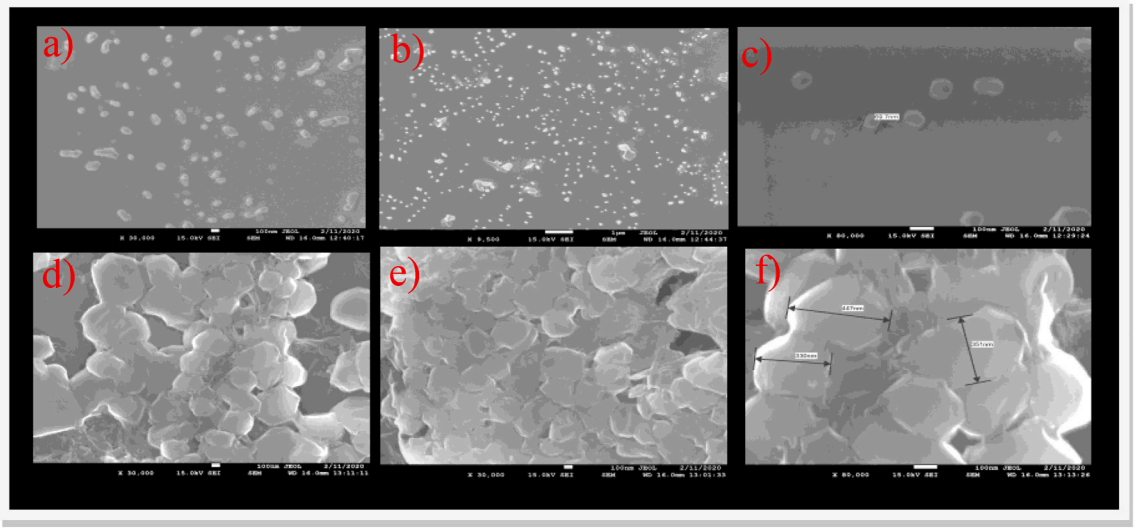

Fig. 4. The SEM picture of **TPP** (a, b), **TPP** + ClO^- (d, e) and zoom SEM image of **TPP** (c) and **TPP** + ClO^- (f).

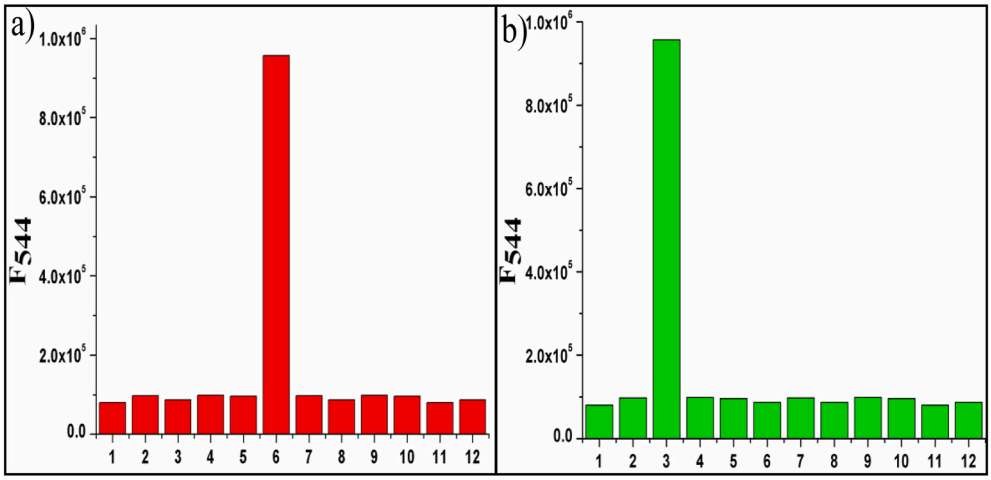

Fig. 5. The fluorescence intensity of probe **TPP** (1.0 μM) in the presence of various analytes (10 equiv.) in PBS buffer solution (pH 7.4, at 25 °C). (a) (1) **TPP**; (2) H_2S (3) CH_3CO_3H (4) NO (5) ONOO− (6) ClO^- (7) $^{\bullet}OH$ (8) $^1O_2$ (9) O^{2-} (10) GSH (11) SO_3^{2-} (12) H_2O_2. (b) (1) **TPP** (2) Al^{3+} (3) ClO^- (4) Co^{2+} (5) Cr^{3+} (6) Cu^{2+} (7) Ni^{2+} (8) Zn^{2+} (9) Cd^{2+} (10) Pb^{2+} (11) Fe^{3+} (12) Hg^{2+}.

cationic (Al^{3+}, Cr^{3+}, Co^{2+}, Cu^{2+}, Ni^{2+}, Cd^{2+}, Zn^{2+}, Pb^{2+}, Fe^{3+}, Hg^{2+}) under biological conditions (Fig. 5b). The results indicated that **TPP** can be employed as a selective fluorescence probe for the sensing of hypochlorite even in the presence of various ROS, RNS and other competitive analytes. Furthermore, a competitive experiment was accomplished to confirm the detection ability of ClO^- in the presence of a large excess (50.0 equiv.) of the other allied analytes ((Fig. S2). The results established that **TPP** showed high selectivity towards ClO^- in physiological conditions (aq. PBS buffer medium) over comparable analytes.

2.7. Effects of the pH

The impact of pH on the fluorescence spectra of **TPP** to hypochlorite in the pH range of 2–12 was thoroughly studied for physiological use.

In the absence of hypochlorite, the **TPP** displayed almost minimal emission variations over the pH range of 2–12. Nonetheless, when hypochlorite was added, the fluorescence intensity of probe **TPP** increased up to pH 6 and subsequently levelled off at pH 8, confirming that **TPP** was suitable for detecting hypochlorite in both weakly acidic and alkaline environment (Fig. 6). This result implies that TPP can working well in biological atmosphere.

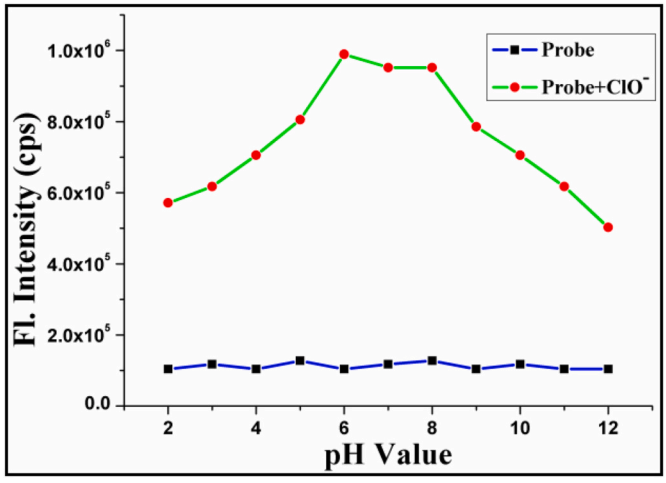

Fig. 6. pH-dependent fluorescence emission response of TPP (10 μM) to ClO− (50 μM) in PBS solution (pH 7.4, 10 μM).

2.8. Sensing mechanism

Turn on response of **TPP** towards ClO^- is due to change in hydrophobicity of the probe due to oxidation of N-methylpyridinium to N-methylpyridone moiety. To validate this, **TPP** was reacted with ClO^- and the reaction product was separated for usual characterization (Figs. S9 and S10). The ^1H NMR spectra of **TPP** and its oxidized adduct were compared (**TPPO**). It is observed that the N-methyl proton in **TPP** resonance at δ 4.42 ppm shifted up field at δ 1.65 ppm due to positive charged nitrogen atom reduced to neutral nitrogen atom (Fig. 7).

The result demonstrated ClO^- promoted oxidation take place and N-methylpyridone derivative is formed (TPPO). Again, mass spectrum analysis was explored to prove the reaction mechanism. As shown in Fig. S5, **TPP** exhibited a peak only at m/z = 451.4690, which corresponds to $[\mathbf{TPP}+H]^+$. However, addition of ClO^-, the initial peak of **TPP** (m/z = 451.4690) completely vanished and a new peak displayed at m/z 466.2173 $[TPPO+H]^+$, which was assigned to N-methylpyridone (TPPO) (Fig. S8).

2.9. Theoretical studies

In order to illuminate the optical phenomenon of **TPP**, DFT and TD-DFT calculations were performed with 6-31G (d, p) basis sets. We observed that HOMO of **TPP** is distributed over tetraphenylethylene moiety while LUMO is located at pyridinium ion (Fig. 8). This result suggests an obvious ICT from tetraphenyl ethylene to pyridinium ion conjugated through π-bond. Agin to know the optical change of **TPP** and **TPPO**, we performed DFT and TDDFT calculated in gas phase. The calculated λ_{max}, oscillator strength (f), main orbital transition, are listed (Tables S2 and SI). Fig. 8 depicts the optimized structures of **TPP** and **TPPO**. The corresponding HOMO-LUMO energy gaps of **TPP** and **TPPO** are 3.1092 eV and 3.4257 eV (Table S2).

There is a substantial alteration in the energy minimisation structure of **TPP** and **TPPO**. In **TPP** alone, the vertical major transition observed at ~386 nm is equivalent to those of the experimentally measured spectra at ~398 nm. The ultimate electronic transition ascends due to HOMO→LUMO (3.1092 eV/398 nm) transition. In case of **TPPO** vertical major transition is similarly HOMO→LUMO (3.4257 eV/309 nm). Extend in energy gap (HOMO→LUMO) in **TPPO** is responsible for blue shift in absorption spectra. And also, the electronic distribution indicates the ICT in **TPP** which in turn interrupted in case of **TPPO**.

2.10. Solid state sensing

Thus, by affording positive findings in the colorimetric/fluorometric sensing of ClO^- in solution phase, its detecting ability has been checked in solid state. For this purpose, Whatman filter paper was exploited to make detection tests more operationally expedient and helpful. **TPP** (1.0 mg/mL) solution in acetonitrile was placed on filter paper and air-dried to produce a simple low-cost solid-state demonstrating strip. After that, dried filter papers were deeped into different concentration of ClO^-. As shown in Fig. 10 fluorescent color of the filter paper strip changes from colorless to yellow upon increasing the concentration of ClO^-. Thus, the preparation of simple test trips can be valued for naked eye detection of ClO^- in a cheap method.

To evaluate the aggregation behavior of **TPP** upon treatment with

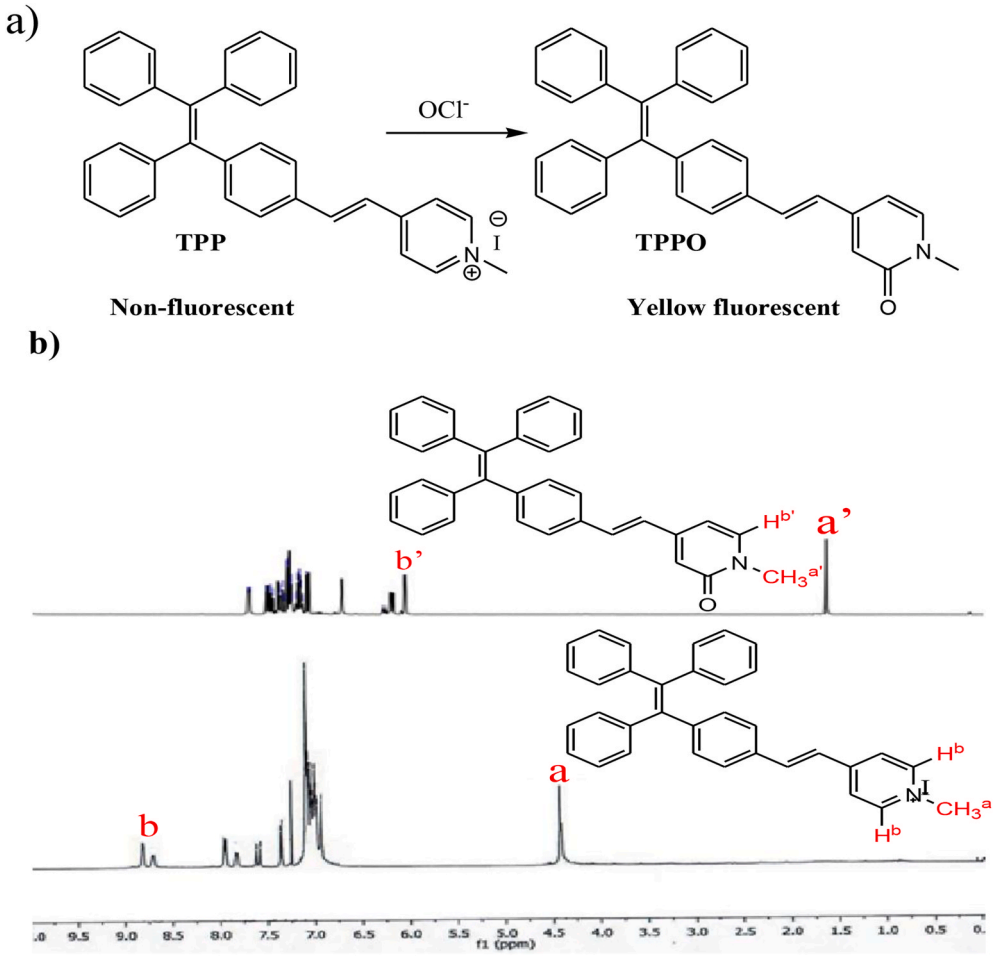

Fig. 7. a) The proposed reaction mechanism. b) Partial ^1H NMR spectra (400 MHz, $CDCl_3$, 25 °C) of **TPP** before and after the addition of ClO^-.

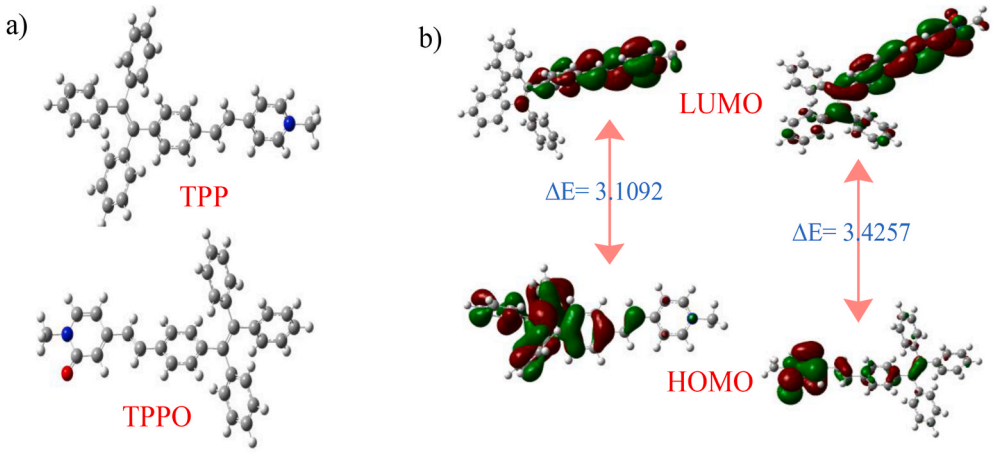

Fig. 8. (a) Energy Optimized structures of **TPP** and **TPPO** (b) HOMO-LUMO distribution and energy difference of **TPP** and **TPPO**.

ClO^-, solid state fluorescence experiment was carried out. Fig. 9 suggests that fluorescence intensity of **TPP** was increased drastically after treatment with ClO^-. Furthermore, we studied the outcome of water volume fraction on the fluorescence of **TPP**. Change of fluorescence of **TPP** was examined in water/DMSO cosolvents with different water volume fractions (fw = 0–90 vol %). Results of these experiments are shown in Fig. S13. Both in a good solvent (fw = 0 vol %) and in a poor solvent (fw = 90 vol %), **TPP** scatters well and displays no fluorescence. These results suggest that **TPP** does not show any AIE behavior. Due to presence of positively charged pyridininium ion, **TPP** in aqueous solution, remains in free molecular state and consequently its hydrophilicity increases. This attributes to its negligible fluorescent intensity in aqueous medium.

Whereas, addition of ClO^- leads to disappearance of positive charge which is accompanied with hydrophobicity of the probe and trigger AIE behavior. In this context, it is not worthy to mention that, in pure organic solvent **TPP** shows a red emissive band at about 630 nm. It is experimented that in pure organic system **TPP** reluctant to sense ClO^-. Whereas, in aqueous PBS buffer solution **TPP** displayed a very low intense emission band at 544 nm which was gradually increased upon concomitant addition of ClO^- due to enhanced AIE behavior.

2.11. Detection of OCl^- in real water samples

After that, we investigated the scenarios for the probe **TPP** to detect ClO^- in various water samples. Because ClO^- is widely used in industrial processes and daily life, there is a risk of the dangerous chemical

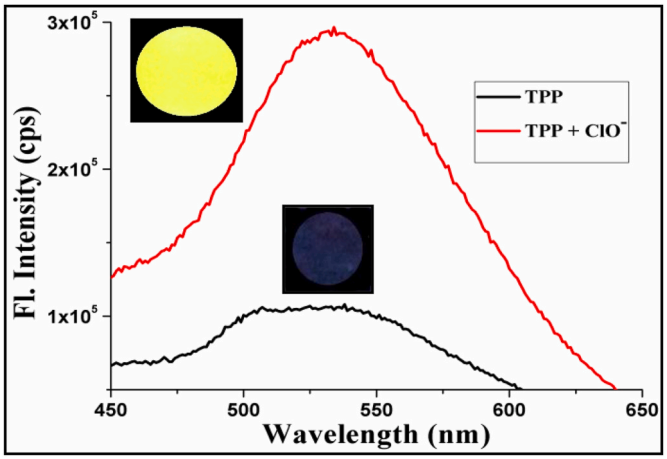

Fig. 9. Solid-state emission of **TPP** in presence and absence of ClO^-.

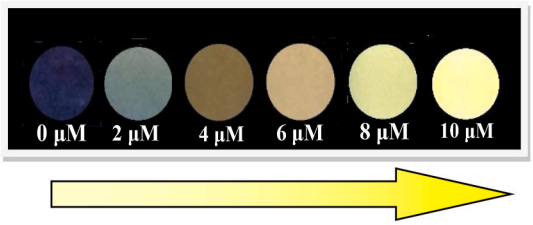

Fig. 10. Filter paper treated with **TPP** (1.0 mg/mL) solution in CH_3CN, with different concentrations of NaClO under UV light.

combining with water. As a result, detecting ClO^- in various water samples is significant for human health. Three water samples with varying concentrations of ClO^- were evaluated in this study. Our process data was consistent with the actual amount of ClO^- added (Table S1). This result shown that **TPP** is capable of quantitatively detecting ClO^- in real-world water samples.

2.12. Biological application

We explored the capability of the probe **TPP** to estimate ClO^- in buffer solution and fetal bovine serum sample. The concentration of the probe **TPP** was sustained at 1.0 μM, whereas ClO^- concentration was varied from 0 to 35 μM. As revealed in Fig. 11 the fluorescence intensity was linearly correlated to ClO^- concentration in the certain concentration range. The regression equation employed was F544 = 3E12 $[ClO^-]$+31,963, with $R^2 = 0.996$ (Fig. 11a). Next, we prepared the fetal bovine serum samples having ClO^- in different concentrations (0–35 μM) and the corresponding regression equation was F544 = 3E12 $[ClO^-]$+51,354, with $R^2 = 0.998$ (Fig. 11b). This relative result suggests that **TPP** could recognize ClO^- in biological systems both qualitatively and quantitatively.

2.13. Cell imaging studies

Due to outstanding fluorescence response of **TPP** toward ClO^- in aqueous solution, we then examined the practical applications of **TPP** to image intracellular ClO^-. For this purpose, two different cell line were chosen e.g. (MG63 (osteosarcoma – human) cancer cells and MC3T3 (osteoblast – mouse) cells). Therefore, in order to achieve this aim, the cytotoxicity of **TPP** and **TPP**+ ClO^- on these living cells must first be evaluated. Thus, traditional MTT assay experiment reveals that both **TPP** and **TPP**+ ClO^- exhibited low cytotoxicity to live MG63 and MC3T3 cells (Fig. S1) up to 15 μM, suggesting that probe is allowable for uses in living organisms.

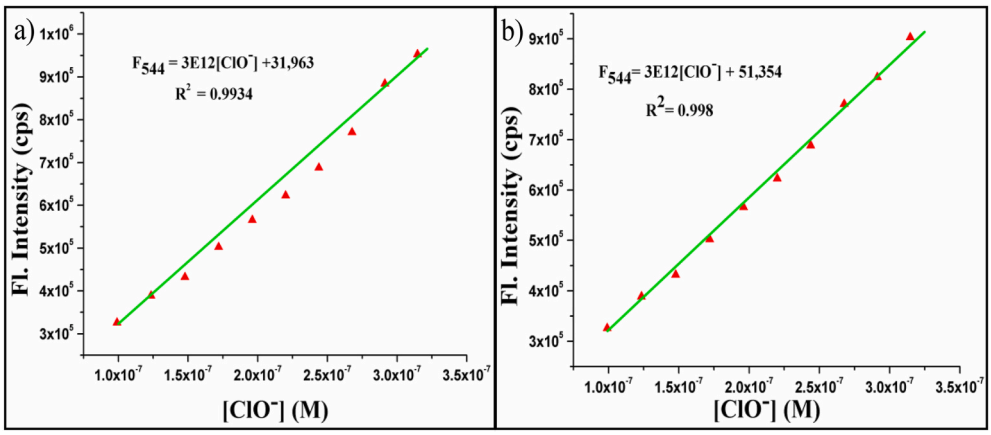

Fig. 11. (a) The relationship between fluorescence intensity and ClO^- concentration in PBS buffer solution (100 mM, pH 7.4, at 25 °C) and (b) in commercial fetal bovine serum.

Initially, MG63 cells were incubated with 1.0 μM **TPP** for 5 min and a yellow fluorescence was exhibited in the intracellular part of the cell. This result confirmed that **TPP** is cell membrane permeable. Much intense yellow fluorescence was observed when 10.0 μM ClO^- was added to the cells which were pretreated with **TPP**. Again, when MG63 cells were pretreated with 10.0 μM of GSH for 20 min followed by incubation of **TPP**, almost no fluorescence was observed (Fig. 12). GSH being a ClO^- scavenger, reduced ClO^- concentration inside cells and thus fluorescence intensity was diminished [70,71]. Thus, increase in fluorescence intensity was due to hypochlorite.

Meanwhile when MC3T3 cells were treated with **TPP** almost no fluorescence was observed, this result agrees well with the phenomenon that cancer cells (MG63) remain under more oxidative stress and also **TPP** can distinguish normal cell from cancer cells. Again, when MC3T3 cells were treated with **TPP** followed by ClO^-, a strong yellow fluorescence was achieved. Furthermore, when MC3T3 cells were incubated with **TPP** and former was pretreated with LPS (1.0 μg/mL) for 1 day followed by PMA (1.0 μg/mL) for 45 min showed yellow fluorescence. LPS/PMA (lipopolysaccharide/phorbol-12-myristate-13- acetate) are responsible for intracellular generation of ClO^- (Fig. 13). The result suggests that **TPP** was capable of detecting endogenous ClO^-.

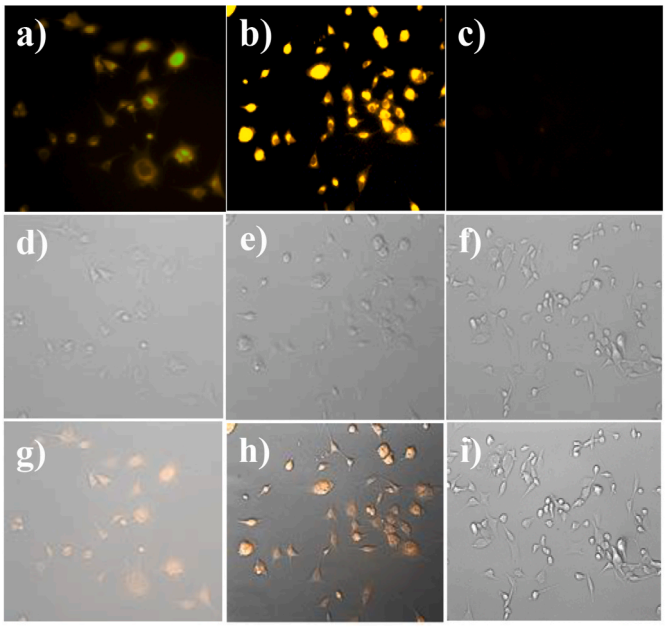

Fig. 12. Fluorescence microscopy images of exogenous ClO^- detection in living MG63 cells using **TPP**. Cells were incubated with (a) **TPP** (1.0 μM) alone for 5 min; (b) **TPP** treated with 10.0 μM ClO^- for 30 min; (C) MG63 cells were pre-treated with GSH (10.0 μM) for 20 min followed by incubation of **TPP** (5.0 μM) for another 30 min; (d) Bright field image of the cells of TPP (1.0 μM) alone; (e) Bright field image of **TPP** treated with 10.0 μM ClO^- for 30 min; (f) Bright field image of the cells were pre-treated with GSH (10.0 μM) for 20 min followed by incubation of **TPP** (5.0 μM) for another 30 min; (g) merged image of **TPP**(1.0 μM) alone; (h) merged image **TPP** treated with 10.0 μM ClO^- for 30 min; (i) merged image of cells were pre-treated with GSH (10.0 μM) for 20 min followed by incubation of **TPP** (5.0 μM) for another 30 min; Emissions were collected at the green channel (500–600 nm) with 380 nm excitation. Scale bar, 20 μm.

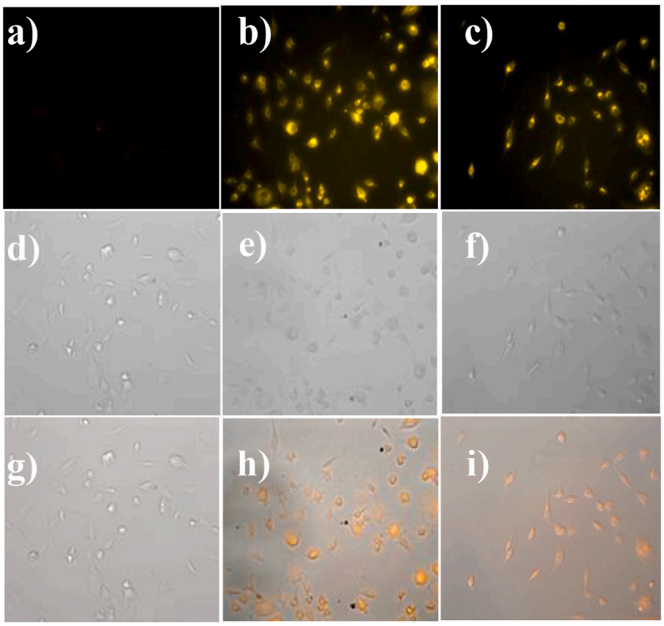

Fig. 13. Fluorescence microscopy images of endogenous ClO^- detection in living MC3T3 cells using **TPP**. Cells were incubated with (a) **TPP** (1.0 μM) alone for 5 min; (b) **TPP** treated with 10.0 μM ClO^- for 30 min; and (C) **TPP** pre-treated with LPS (1.0 μg) for 1 day followed by PMA for 45 min; (d) Bright field image of the cells of **TPP** (1.0 μM) alone; (e) Bright field image of **TPP** treated with 10.0 μM ClO^- for 30 min; (f) Bright field image of **TPP** pretreated with LPS (1.0 μg) for 1 day followed by PMA for 45 min; (g) merged image of the cells of **TPP** (1.0 μM) alone; (h) merged image of **TPP** treated with ClO^- for 30 min; (i) merged image of **TPP** pretreated with LPS (1.0 μg) for 1 day followed by PMA for 45 min; Emissions were collected at the green channel (500–600 nm) with 380 nm excitation. Scale bar, 20 μm.

3. Conclusion

In summary, we have reported an AIE-active "turn-on" fluorescent chemodosimeter **TPP** for the detection of ClO^- in PBS buffer solution and living cells. In presence of ClO^-, chemodosimeter **TPP** exhibited ratiometric absorption changes along with notable fluorescent enhancement (10-fold) due to the oxidation of N-alkylpyridinium part to N-methyl-2-pyridone moiety. This chemodosimeter displayed quick reaction time (10s), high selectivity towards ClO^- over other competing analytes (ROS, RNS, other interfering ions), ensuring the specificity required for any real implementation. In addition, the scanning electron microscopy (SEM) results indicated a change in morphology from spherical to aggregates upon addition of ClO^- to the buffer solution of **TPP**. Furthermore, test kit experiments demonstrated that **TPP** can be employed for the solid-state sensing of ClO^- in environments. It is particularly able to measure the ClO^- concentration in fetal bovine serum samples and a wide range of real water samples, implying a variety of useful applications. Moreover, cell membrane permeable probe **TPP** can be successfully used for the detection of intracellular ClO^- in living MG63 (osteosarcoma – human) cancer cells and MC3T3 (osteoblast – mouse) cells with very low cytotoxicity. Importantly, the probe can distinguish between cancer cells and normal animal cells quite efficiently. Therefore, we hope that our chemodosimeter will be of interest to scientists investigating the various activities of ClO^- in environmental and biological systems.

CRediT authorship contribution statement

Sandip Kumar Samanta: Study conception and design, Data collection, Formal analysis and interpretation of results, Draft manuscript, preparation. **Kalipada Maiti:** Study conception and design, Data collection, Formal analysis and interpretation of results, Draft manuscript, preparation. **Saikat Kumar Manna:** Data collection, Formal analysis and interpretation of results, Draft manuscript, preparation. **Syed Samim Ali:** Data collection, Formal analysis and interpretation of results. **Uday Narayan Guria:** Data collection, Formal analysis and interpretation of results. **Aritri Ghosh:** Data collection, Formal analysis and interpretation of results. **Pallab Datta:** Data collection, Formal analysis and interpretation of results,. **Ajit Kumar Mahapatra:** Study conception and design, Formal analysis and interpretation of results, Draft manuscript, preparation, All authors reviewed the results and approved the final version of the manuscript.

Declaration of competing interest

The authors declare that they have no known competing financial interests or personal relationships that could have appeared to influence the work reported in this paper.

Acknowledgements

We gratefully acknowledge the CSIR-New Delhi [File No. 02(0334)/18/EMR-II] for financial support. SKS thanks UGC, New Delhi, India for a fellowship.

Appendix A. Supplementary data

Supplementary data to this article can be found online at https://doi.org/10.1016/j.dyepig.2021.109758.

References

[1] Skulachev VP, Anisimov VN, Antonenko YN, Bakeeva LE, Chernyak BV, Erichev VP, Filenko OF, Kalinina NI, Kapelko VI, Kolosova NG, Kopnin BP, Korshunova GA, Lichinitser MR, Obukhova LA, Pasyukova EG, Pisarenko OI, Roginsky VA, Ruuge EK, Senin I Severina, Skulachev MV, Spivak IM, Tashlitsky VN, Vsevolod A, Tkachuk o, Yu Mikhail, Vyssokikh a, Lev S, Yaguzhinsky a, Zorov Dmitry B. An attempt to prevent senescence: a mitochondrial approach. Biochim Biophys Acta 2009;1787:437–61.
[2] Morris AA, Zhao L, Patel RS, Jones DP, Ahmed Y, Stoyanova N, Gibbons GH, Vaccarino V, Din-Dzietham R, Quyyumiet AA. Differences in systemic oxidative stress based on race and the metabolic syndrome: the morehouse and emory team up to eliminate health disparities (meta-health) study. Metab Syndr Relat Disord 2012;10:252–9.
[3] Kander MC, Cui Y, Liu Z. Gender difference in oxidative stress: a new look at the mechanisms for cardiovascular diseases. J Cell Mol Med 2017;21:1024–32.
[4] Janicki-Deverts D, Cohen S, Matthews KA, Gross MD, Jacobs Jr DR. Socioeconomic status, antioxidant micronutrients, and correlates of oxidative damage: the coronary artery risk development in young adults (CARDIA) study. Psychosom Med 2009;71:541–8.
[5] King GL, Loeken MR. Hyperglycemia-induced oxidative stress in diabetic complications. Histochem Cell Biol 2004;122:333–8.
[6] Chen X, Wang F, Hyun JY, Wei T, Qiang J, Ren X, Shin I, Yoon JY. Recent progress in the development of fluorescent, luminescent and colorimetric probes for detection of reactive oxygen and nitrogen species. Chem Soc Rev 2016;45:2976–3016.
[7] Yang Y, Zhao Q, Feng W, Li F. Luminescent chemodosimeters for bioimaging. Chem Rev 2013;113:192–270.
[8] Xing P, Gao K, Wang B, Gao J, Yan H, Wen J, Li W, Xu Y, Li H, Chen J, Wang W, Sun S. HEPES is not suitable for fluorescence detection of HOCl: a noval probe for HOCl in absolute PBS. Chem Commun 2016;28:5064–6.
[9] Kang J, Huo F, Yue Y, Wen Y, Chao J, Zhang Y, Yin C. A solvent depend on ratiometric fluorescent probe for hypochlorous acid and its application in living cells. Dyes Pigments 2017;136:852–8.
[10] Huang Y, Zhang P, Gao M, Zeng F, Qin A, Wu SZ, Tang BZ. Ratiometric detection and imaging of endogenous hypochlorite in live cells and in vivo achieved by using an aggregation induced emission (AIE)-based nanoprobe. Chem Commun 2016;52:7288–91.
[11] Zhang YR, Meng N, Miao JY, Zhao BX. A ratiometric fluorescent probe based on a through-bond energy transfer (TBET) system for imaging HOCl in living cells. Chem – Eur J 2015;21:19058–63.
[12] Wang Y, Wu L, Liu CY, Guo BP, Zhu BC, Wang ZK, Duan QX, Ma ZM, Zhang XL. A highly specific and ultrasensitive fluorescent probe for basal lysosomal HOCl detection based on chlorination induced by chlorinium ions (Cl^+). J Mater Chem B 2017;5:3377–82.
[13] Sugiyama S, Okada Y, Sukhova GK, Virmani R, Heinecke JW, Libby P. Macrophage myeloperoxidase regulation by granulocyte macrophage colony-stimulating factor in human atherosclerosis and implications in acute coronary syndromes. Am J Pathol 2001;158:879–91.
[14] Malle E, Buch T, Grone HJ. Myeloperoxidase in kidney disease. Kidney Int 2003;64:1956–67.
[15] Hammerschmidt S, Büchler N, Wahn H. Tissue lipid peroxidation and reduced glutathione depletion in hypochlorite-induced lung injury. Chest 2002;121:573–81.
[16] Yap YW, Whiteman M, Cheung NS. Chlorinative stress: an underappreciated mediator of neurodegeneration. Cell Signal 2007;19:219–28.
[17] Steinbeck MJ, Nesti LJ, Sharkey PF, Parvizi J. Myeloperoxidase and chlorinated peptides in osteoarthritis: potential biomarkers of the disease. J Orthop Res 2007;25:1128–35.
[18] Güngör N, Knaapen AM, Munnia A, Peluso M, Haenen GR, Chiu RK, Godschalk RWL, Schooten FJV. Genotoxic effects of neutrophilis and hypochlorous acid. Mutagenesis 2010;25:149–54.
[19] Harrison JE, Schultz J. Studies on the chlorinating activity of myeloperoxidase. J Biol Chem 1976;251:1371.
[20] Harrison EJ, Schultz J. Studies on the chlorinating activity of myeloperoxidase. J Biol Chem 1976;254:1371–4.
[21] Tanenbaum ME, Gilbert LA, Qi LS, Weissman JS, Vale RD. A protein-tagging system for signal amplification in gene expression and fluorescence imaging. Cell 2014;159:635–46.
[22] Chan J, Dodani SC, Chang CJ. Reaction-based small-molecule fluorescent probes for chemoselective bioimaging. Nat Chem 2012;4:973–84.
[23] Yuan L, Lin W, Zheng K, He L, Huang W. Far-red to near infrared analyte-responsive fluorescent probes based on organic fluorophore platforms for fluorescence imaging. Chem Soc Rev 2013;42:622–61.
[24] Li X, Gao X, Shi W, Ma H. Design strategies for water-soluble small molecular chromogenic and fluorogenic probes. Chem Rev 2014;114:590–659.
[25] Duan C, Won M, Verwilst P, Xu J, Kim HS, Zeng L, Kim JS. In vivo imaging of endogenously produced HClO in zebrafish and mice using a Bright, photostable ratiometric fluorescent probe. Anal Chem 2019;91:4172–8.
[26] Yin C, Zhu H, Xie C, Zhang L, Chen P, Fan Q, Huang W, Pu K. Organic nanoprobe cocktails for multicolor fluorescence imaging of reactive oxygen species. Adv Funct Mater 2017;27:1700493.
[27] Feng H, Zhang Z, Meng Q, Jia H, Wang Y, Zhang R. Rapid response fluorescence probe enabled in vivo diagnosis and assessing treatment response of hypochlorous acid-mediated rheumatoid arthritis. Adv Sci 2018;5:1800397.
[28] Duan Q, Jia P, Zhuang Z, Liu C, Zhang X, Wang Z, Sheng W, Li Z, Zhu H, Zhu B, Zhang X. Rational design of a hepatoma-specific fluorescent probe for HOCl and its bioimaging applications in living HepG2 cells. Anal Chem 2019;91:2163–8.
[29] Pak YL, Park SJ, Xu Q, Kim HM, Yoon J. Ratiometric two-photon fluorescent probe for detecting and imaging hypochlorite. Anal Chem 2018;90:9510–4.
[30] Pak YL, Park SJ, Wu D, Cheon B, Kim HM, Bouffard J, Yoon J. N-heterocyclic carbene boranes as reactive oxygen species-responsive materials: application to the

two-photon imaging of hypochlorous acid in living cells and tissues. Angew Chem Int Ed 2018;57:1567–71.
[31] Jiao X, Xiao Y, Li Y, Liang M, Xie X, Wang X, Tang B. Evaluating drug-induced liver injury and its remission via discrimination and imaging of HOCl and H_2S with a two-photon fluorescent probe. Anal Chem 2018;90:7510–6.
[32] Ren M, Li Z, Deng B, Wang L, Lin W. Single fluorescent probe separately and continuously visualize H_2S and HOCl in lysosomes with different fluorescence signals. Anal Chem 2019;91:2932–8.
[33] Zhang X, Zhao W, Li B, Li W, Zhang C, Hou X, Jiang J, Dong Y. Ratiometric fluorescent probes for capturing endogenous hypochlorous acid in the lungs of mice. Chem Sci 2018;9:8207–12.
[34] Zhang R, Zhao J, Han G, Liu Z, Liu C, Zhang C, Liu B, Jiang C, Liu R, Zhao T, Han MY, Zhang ZJ. Real-time discrimination and versatile profiling of spontaneous reactive oxygen species in living organisms with a single fluorescent probe. Am Chem Soc 2016;138:3769–78.
[35] Wu D, Chen L, Xu Q, Chen X, Yoon J. Design principles, sensing mechanism and application of highly specific fluorescent probes for HOCl/OCl^-. Acc Chem Res 2019;52:2158–68.
[36] Wang S, Zhu B, Wang B, Cao X, Zhu L, Zeng L. Revealing HOCl burst from endoplasmic reticulum in cisplatin-treated cells via a ratiometric fluorescent probe. Chin Chem Lett 2021;32:1795–8.
[37] Hou JT, Kim HS, Duan C, Ji MS, Wang S, Zeng L, Ren WX, Kim JS. A ratiometric fluorescent probe for detecting hypochlorite in the endoplasmic reticulum. Chem Commun 2019;55:2533–6.
[38] Li Y, Wang W, Zhuang Z, Wang Z, Lin G, Shen P, Chen S, Zhao Z, Tang BZ. Efficient red AIEgens based on tetraphenylethylene: synthesis, structure, photoluminescence and electroluminescence. J Mater Chem C 2018;6:5900–7.
[39] Luo J, Xie Z, Lam JWY, Cheng L, Chen H, Qiu C, Kwok HS, Zhan X, Liu Y, Zhu D, Tang BZ. Aggregation-induced emission of 1-methyl-1,2,3,4,5-pentaphenylsilole. Chem Commun 2001:1740.
[40] Zhao Z, Wang Z, Lu P, Chan CYK, Liu D, Lam JWY, Sung HHY, Ian DW, Ma Y, Tang BZ. Structural modulation of solid-state emission of 2, 5-bis (trialkylsilylethynyl)-3, 4-diphenylsiloles. Angew Chem Int Ed 2009;48:7608.
[41] Zhao Z, He B, Tang BZ. Aggregation-induced emission of siloles. Chem Sci 2015;6:5347.
[42] Li Q, Li Z. The strong light-emission materials in the aggregated state: what happens from a single molecule to the collective group. Adv Sci 2017;4:1600484.
[43] Zhong X, Yang Q, Chen Y, Jiang Y, Wang B, Shen J. A mitochondria-targeted fluorescent probe based on coumarin–pyridine derivatives for hypochlorite imaging in living cells and zebrafish. J Mater Chem B 2019;7:7332–7.
[44] Wu Y, Wang J, Zeng F, Huang S, Huang J, Xie H, Yu C, Wu S. Pyrene derivative emitting red or near-infrared light with monomer/excimer conversion and its application to ratiometric detection of hypochlorite. ACS Appl Mater Interfaces 2016;8:1511–9.
[45] Kenmoku S, Urano Y, Kojima H, Nagano T. Development of a highly specific rhodamine-based fluorescence probe for hypochlorous acid and its application to real-time imaging of phagocytosis. J Am Chem Soc 2007;129:7313–8.
[46] Koide Y, Urano Y, Hanaoka K, Terai T, Nagano T. Development of an Si-Rhodamine-Based far-red to near-infrared fluorescence probe selective for hypochlorous acid and its application for biological imaging. J Am Chem Soc 2011;133:5680–2.
[47] Best QA, Sattenapally N, Dyer DJ, Scott CN, McCarroll ME. pH-dependent Si-fluorescein hypochlorous acid fluorescent probe: spirocycle ring-opening and exess hypochlorous acid-induced chlorination. J Am Chem Soc 2013;135:13365–70.
[48] Zhao Yun, Xue Y, Sun J, Xuan H, Xu Y, Cui Y, Dong J. A new red fluorescent probe based on rosamine-phenothiazine for the highly selective and rapid detection of hypochlorite and its bioimaging in live cells. New J Chem 2020;44:12674–9.
[49] Gong J, Liu C, Cai S, He S, Zhao L, Zeng X. Nove l near-infrared fluorescent probe with a large Stokes shift for sensing hypochlorous acid in mitochondria. Org Biomol Chem 2020;18:7656–62.
[50] Wen X, Yan L, Fan Z. One-step construction of a novel AIE probe based on diaminomaleonitrile and its application in double-detection of hypochlorites and formaldehyde gas. New J Chem 2021;45:8155–65.
[51] Zhong X, Yang Q, Chen Y, Jiang Y, Dai Z. Aggregation-induced fluorescence probe for hypochlorite imaging in mitochondria of living cells and zebrafish. J Mater Chem B 2020;8:7375–81.
[52] Zhang P, Zhang Q, Li S, Chen W, Guo X, Ding CS, Urano Y, Kojima H, Nagano T. Enhanced fluorescence sensing of hypochlorous acid using serum albumin as a signal amplifier. Mater Chem B 2019;7:1238–45.
[53] Sun Z, Liu F, Chen Y, Tam PKH, Yang D. A highly specific BODIPY-based fluorescent probe for the detection of hypochlorous acid. Org Lett 2008;10:2171–4.
[54] Zhang W, Guo C, Liu L, Qin J, Yang C. Naked-eye visible and fluorometric dual-signalling chemodosimeter for hypochlorous acid based on water-soluble p-methoxyphenol derivative. Org Biomol Chem 2011;9:5560–3.
[55] Wang Z, Zhang Y, Song J, Li M, Yang Y, Xu x, Xu H, Wang S. Three noval camphor-based fluorescence probes for ratiometric detection of hypochlorite and bio-imaging in living cells. Sens Actuators B 2019;284:148–58.
[56] Wu G, Zeng F, Wu S. A water-soluble and specific BODIPY-based fluorescent probe for hypochlorite detection and cell imaging. Anal Methods 2013;5:5589–96.
[57] Cheng X, Jia H, Long T, Feng J, Qin J, Li Z. A "turn-on" fluorescent probe for hypochlorous acid: convenient synthesis, good sensing performance and strategy by the removal of C=N isomerization. Chem Commun 2011;47:11978–80.
[58] Zhang Q, Zhang P, Gong Y, Ding C. Two-photon AIE based fluorescent probe with large Stokes shift for selective and sensitive detection and visualization of hypochlorite. Sens Actuators B 2019;278:73–81.
[59] Wu Y, Wang J, Zeng F, Huang S, Huang J, Xie H, Yu C, Wu S. Pyrene derivative emitting red or near-infrared light with monomer/excimer conversion and its application to ratiometric detection of hypochlorite. ACS Appl Mater Interfaces 2016;8:1511–9.
[60] Wang L, Chen X, Xia Q, Liu R, Qu J. Deep-red AIE-active fluorophore for hypochlorite detection and bioimaging in live cells. Ind Eng Chem Res 2018;57:7735–41.
[61] Han X, Ma Y, Chen Y, Wang X, Wang Z. Enhancement of the aggregation-induced emission by hydrogen bond for visualizing hypochlorous acid in an inflammation model and a hepatocellular carcinoma model. Anal Chem 2020;92:2830–8.
[62] Qian J, Tang BZ. AIE luminogens for bioimaging and theragnostic: from organelles to animals. Inside Chem 2017;3:56–91.
[63] Zhao X, Chen Y, Niu G, Gu D, Wang J, Cao Y, Yin Y, Li X, Ding D, Xi R, Meng M. Photostable pH-sensitive near-infrared aggregation-induced emission luminogen for long-term mitochondrial tracking. ACS Appl Mater Interfaces 2019;11:13134–9.
[64] Hou Y, Li Z, Hou J, Shi P, Li Y, Niu M, Liu Y, Han T. Conditional mechanochromic fluorescence with turn-on response: a new way to encrypt and decrypt binary data. Dyes Pigments 2018;149:253–60.
[65] Nolan EM, Ryu JW, Jaworski J, Feazell RP, Sheng M, Lippard SJ. Zinspy sensors with enhanced dynamic range for imaging neuronal cell zinc uptake and mobilization. J Am Chem Soc 2006;128:15517.
[66] Dodani SC, Leary SC, Cobine PA, Winge DR, Chang CJ. A targetable fluorescent sensor reveals that copper-deficient *SCO1* and *SCO2* patient cells prioritize mitochondrial copper homeostasis. J AmChem Soc 2011;133:8606.
[67] Zeng L, Chen T, Chen BQ, Yuan HQ, Sheng R, Bao GM. A distinctive mitochondrion-targeting, in situ-activatable near-infrared fluorescent probe for visualizing sulfur dioxide derivatives and their fluctuations in vivo. J Mater Chem B 2020;8:1914–21.
[68] Gupta AS, Paul K, Luxami V. A fluorescent probe with "AIE + ESIPT" characteristics for Cu^{2+} and F^- ions estimation. Sensor Actuator B 2017;246:653–61.
[69] Pramanik S, Bhalla V, Kim HM, Singh H, Lee HW, Kumar M. A hexaphenylbenzene based AIEE active two photon probes for the detection of hydrogen sulfide with tunable self-assembly in aqueous media and application in live cell imaging. Chem Commun 2015;51:15570–3.
[70] Qiao L, Nie H, Wu Y, Xin F, Gao C, Jing J, Zhang X. An ultrafast responsive BODIPY-based fluorescent probe for the detection of endogenous hypochlorite in live cells. J Mater Chem B 2017;5:525.
[71] Haenen GRMM, Bast A. Glutathione revisited: a better scavenger than previously thought. Front Pharmacol 2014;5:260.